Crystal structure and high temperature tribological behavior of niobium aluminum nitride films

Article *in* Materialia · August 2018

DOI: 10.1016/j.mtla.2018.08.025

6 authors, including:

Hongbo Ju
Jiangsu University of Science and Technology
62 PUBLICATIONS **958** CITATIONS

SEE PROFILE

Materialia 3 (2018) 202–211

Contents lists available at ScienceDirect

Materialia

journal homepage: www.elsevier.com/locate/mtla

Full Length Article

Crystal structure and high temperature tribological behavior of niobium aluminum nitride films

Hongbo Ju[a,c,*], Pei Jia[a], Junhua Xu[a,b,*], Lihua Yu[a,**], Isaac Asempah[a], Yaoxiang Geng[a]

[a] School of Materials Science and Engineering, Jiangsu University of Science and Technology, Mengxi Road 2, Zhenjiang, Jiangsu Province 212003, China
[b] National Demonstration Center for Experimental Materials Science and Technology, Jiangsu University of Science and Technology, Mengxi Road 2, Zhenjiang, Jiangsu Province 212003, China
[c] Yangzijiang Shipbuilding (Holdings) Ltd., 1# lianyi Road, Jiangyin-Jingjiang Industry Zone, Jingjiang, Jiangsu Province, China

ARTICLE INFO

Keywords:
Reactive magnetron sputtering
Niobium aluminum nitride films
Tribological behavior

ABSTRACT

Niobium aluminum nitride (Nb–Al–N) films with various aluminum content were deposited using a reactive magnetron system and the film with 22.3 at% aluminum exhibiting the highest hardness, lowest wear rate and friction coefficient at room temperature was chosen to investigate the tribological properties at elevated testing temperatures. The results showed that from room temperature to 200 °C, the absence of oxide-based tribo-phases led to the reduction in wear rate, but friction coefficient remained stable. As the testing temperature increased from 200–500 °C, there was reemergence of γ-alumina tribo-phase, this resulted in intensified interaction between the wear track and the counterpart leading to an increase in both the wear rate and friction coefficient. A further increase in testing temperature resulted in a phase transition from a porous γ-alumina to a dense α-alumina. This transition aided in the reconstruction of the worn area in the wear track and the improvement in the friction and wear resistance properties.

1. Introduction

The research on the tribological properties of materials is critical in surface engineering. Improving the wear and frictional properties of materials started in ancient times and have been pursued until now. The fabrication of lubricating material with improved properties have received a lot of attention in recent times due to increase in awareness of protecting the environment, fuel economy and depleting oil resources [1,2]. Transition metal nitride (TMN) films with excellent mechanical and tribological properties are widely applied in the cutting tools to prolong its service life [3–6]. In recently years, niobium nitride based films were considered as one of candidate materials in cutting tools due to some unique properties such as high hardness, good wear resistant, thermal expansion coefficient matching to tool steels [7–9]. Improvement of the mechanical and tribological properties at room temperature and elevated temperature is driving force for further development of niobium nitride based films. Studies have shown that the addition of elements such as aluminum [10], titanium [11], silver [12], yttrium [3] and silicon [3,13] to form a ternary thin film could improve the properties of TMN films. For example, the addition of aluminum into titanium nitride matrix film to form a single-phase face-centered cubic titanium aluminum nitride can significantly improve the oxidation resistance and mechanical properties [14]. A similar effect of aluminum was also reported in other TMN systems such as zirconium aluminum nitride [15,16] and niobium aluminum nitride [17,18].

A dense alumina formed on the surface of the aluminum-containing TMN films was considered as an effective diffusion barrier which resulted in the improvement of the thermal stability of the film [19–21]. The incorporation of aluminum into Mo2N binary film can reduce the tensile and shear stress induced by the counterpart, thereby improving the tribological properties of molybdenum aluminum nitride films during wear test [19]. Recently, Ivashchenko et al. [17] deposited niobium aluminum nitride system with different aluminum content using magnetron sputtering and discussed the relationship between the phase transition and mechanical properties in detail. However, the influence of aluminum content on the tribological properties of the film, especially at elevated temperatures have not been studied thoroughly.

In this work, series of niobium aluminum nitride composite films with different aluminum content were deposited using reactive magnetron sputtering, and the influence of aluminum content on the microstructure, mechanical and tribological properties at room temperature (RT) was studied. Films with excellent mechanical and tribological

* Correspondent authors at: School of Materials Science and Engineering, Jiangsu University of Science and Technology, Mengxi Road 2, Zhenjiang, Jiangsu Province 212003, China
** Correspondent author.
E-mail addresses: hbju@just.edu.cn (H. Ju), jhxu@just.edu.cn (J. Xu), lhyu6@just.edu.cn (L. Yu).

https://doi.org/10.1016/j.mtla.2018.08.025
Received 11 May 2018; Received in revised form 24 August 2018; Accepted 26 August 2018
Available online 28 August 2018

properties at RT were chosen, and their tribological behavior over a wide testing temperature range was investigated.

2. Experiment

Niobium aluminum nitride (Nb–Al–N) films with a thickness of about 2 μm were deposited on both polished stainless-steel (AISI 304 SS, 192 H_v) and Si (100) wafer substrates using a multi-target magnetron sputtering system. Before the deposition of the films onto the substrates, the stainless-steel and silicon (100) were first rinsultrasonically in acetone for 10 min and subsequently rinsed in ethanol for the same period. It was then mounted onto a substrate holder in the chamber after blow-drying. The distance of target-to-substrate was 90 mm. After a base pressure of 6.0×10^{-4} Pa was attained, surface contaminants on the niobium (99.9 %, Ø 75 mm) and aluminum (99.9 %, Ø 75 mm) targets were removed through argon bombardment with target power of 40 W. The power of the niobium target was subsequently increased to 150 W with a substrate temperature of 200 ˚C for the deposition of a 100 nm niobium adhesion layer onto the substrates. Various Nb–Al–N films with a thickness of ~2 μm were deposited by fixing the niobium target power to 280 W and adjusting the power of the Aluminum target from 0 to 150 W while continually maintaining the working pressure at 0.3 Pa with a nitrogen to argon ratio (flow ratio) of 10:5. Besides this, no substrate bias was applied during the deposition. The Nb–Al–N deposited on the mirror polished stainless-steel substrates were used for the evaluation of the film's resistance to wear, whereas the samples deposited on the silicon (100) wafer were used to evaluate the film's compositional, structural, thermal and mechanical properties.

The elemental compositions of the films were determined by energy dispersive spectroscopy (EDS) on an EDAX DX-4 energy dispersive analyzer. The microstructure of the films was evaluated using a Siemens X-ray diffractometer with Cu Kα radiation, operated at 40 kV, 35 mA. Calculation of the grain size was done by using the Debye–Scherrer's equation. High-resolution transmission electron microscopy (HRTEM) was performed using a JEOL JEM-2100F microscope operated at an accelerating voltage of 200 kV. The oxidation resistance of the films was measured by a thermogravimetry (TG) system (SDT-2960, TA Instrument) equipped with a thermogravimetric unit. The samples were heated from 200 ˚C to 1200 ˚C at a heating rate of 15 ˚C/min and 60 ml/min of air to maintain an oxidative atmosphere for the thermal decomposition. Calculation of the residual stress (σ) was done using data obtained from Bruker DEKTAK-XT profilometer and applying Stoney's equation [2]. A nano-indentation tester system (nano-indenter CPX+NHT+MST), equipped with a diamond Berkovich indenter tip was used to determine the hardness, elastic modulus and the adhesion force of the film. The indenter was calibrated using fused silica as a reference. A maximum load of 4 mN was applied to meet the criterion that the indention depth is less than 10% of the film thickness, and a total of nine (9) indentations were made for each sample and the mean value taken. The value of the Poison ratio for the calculation of elastic modulus for the films was 0.3. The UMT-2 high-temperature tribometer with Si_3N_4 ceramic ball counterpart (diameter of 9.38 mm, a hardness of ~12 GPa) was used in carrying out the wear test. The counterpart was first rinsed ultrasonically in acetone for 5 min and subsequently rinsed in ethanol for the same period before the wear test. With a spindle velocity of 50 r/min, a circular track of 8 mm, a 30-min wear test was performed at various temperatures (room temperature (RT), 200, 400, 500, 600, 700 and 800 ˚C). The relative humidity for the RT test was 40 ± 5%. The electric resistance furnace equipped on the tribometer was heated at a rate of 15 ˚C/min for the performance of the high-temperature wear test. Each test was performed three times, and the average values used to reduce errors. Raman spectroscopy was performed on the wear track to measure the tribo-film therein. By utilizing surface profilometer and taking mean values along the wear track, the wear rate (*WR*) of the films was calculated according to Archard's classical wear equation.

Table 1
Chemical compositions of the Nb–Al–N films as a function of aluminum target power.

	Chemical compositions (at%)			
v	Niobium	Aluminum	Nitrogen	Oxygen
0	51.0 ± 2.6	0.0	46.7 ± 2.3	2.3 ± 0.1
30	43.3 ± 2.2	7.4 ± 0.4	47.1 ± 2.4	2.2 ± 0.1
60	29.0 ± 1.5	22.3 ± 1.1	46.6 ± 2.3	2.1 ± 0.1
90	22.1 ± 1.1	29.0 ± 1.5	46.5 ± 2.3	2.4 ± 0.1
120	16.0 ± 0.8	34.1 ± 1.7	47.7 ± 2.4	2.2 ± 0.1
150	11.0 ± 0.6	38.3 ± 1.9	48.3 ± 2.4	2.4 ± 0.1

3. Results and discussion

3.1. Crystal structure

Table 1 shows the chemical compositions of niobium aluminum nitride (Nb–Al–N) films as a function of aluminum target power. As shown in Table 1, the aluminum content in the films increases gradually from 0 at% to 38.3 at% with an increase in the aluminum target power from 0 W to 150 W, there is a decrease in the niobium content from 51.0 at% to 11.0 at% as a result. Both nitrogen and oxygen content in the films are not influenced by the aluminum target power significantly, and their values remain at ~47.0 at% and ~2.2 at%, respectively.

The effect of aluminum content on the crystal structure was studied using XRD, and the results are shown in Fig. 1(a). Fig. 1(b) is the enlarged XRD pattern of the film with 29.0 at% aluminum. As shown in Fig. 1, the binary niobium nitride film exhibits a two-phase structure where a face-centered cubic (fcc) NbN (JCPDF card 38-1155) and hexagonal close-packed (hcp) NbN (JCPDF card 14-0547) coexists in the film. This result is similar to that in Ref. [8]. Fig. 1(a) also illustrates the XRD pattern of aluminum nitride film synthesized under the same condition used as a comparison, and the result shows that the binary aluminum nitride film presents a single hcp-AlN phase (JCPDF card 25-1133). The ternary Nb–Al–N films with aluminum content <22.3 at% aluminum still exhibits four peaks similar to that of niobium nitride film and no diffraction peaks corresponding to aluminum nitride were observed. However, a further increase in aluminum content to 29.0at% induces other two diffraction peaks at ~34˚ and ~37˚ apart from the four niobium nitride peaks and the two peaks correspond to hcp-AlN (100) and (101), respectively. The incorporation of aluminum above 29.0 at% into the niobium nitride matrix leads to the disappearance of the fcc-NbN (111) diffraction peak. This demonstrates that a three-phase consisting of fcc-NbN, hcp-NbN and hcp-AlN co-exists in the Nb–Al–N films when the aluminum content is >22.3 at% aluminum.

To further elaborate the crystal structure of Nb–Al–N films, transmission electron microscopy (TEM) was carried out, the TEM images along with its corresponding selected area electron diffraction (SAED) pattern are presented in Figs. 2 and 3. The Nb–Al–N film with an aluminum content of 22.3 at% in Fig. 2(a) revealed that the film had a dense columnar structure and the width of the column is ~100 nm. As shown in Fig. 2(b), the SAED pattern of the film exhibits a double phase of fcc-NbN and hcp-NbN; the diffraction rings can be referred to as the lattice planes of hcp-NbN (101) and fcc-NbN (200), (220) from inner to outer. Fig. 2(c) is the HRTEM image of the film and its corresponding Fast Fourier Transform (FFT) and Inverse Fast Fourier Transform (IFFT) (shown as inset). As shown in Fig. 2(c), two types of lattice spacing with the value of 0.2528 and 0.2187 nm are detected, and they correspond to fcc-NbN (111) and (200) based on the JCPDF card 38-1155. The lattice spacing of the above lattice fringes is smaller than the standard lattice spacing, this suggests, that the film lattice is influenced by smaller aluminum atoms which replace niobium atoms in niobium nitride lattice. The fcc-NbN (111) and (200) planes appear in the FFT pattern, and the angle between the two planes is 54˚. Increasing the aluminum content to 29.0 at% has a little influence on the columnar structure and the col-

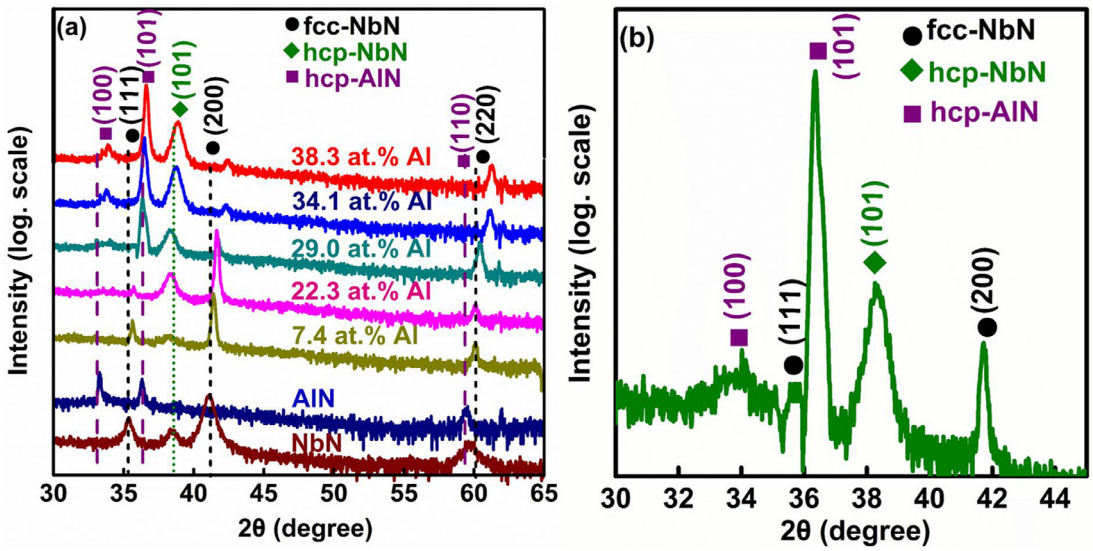

Fig. 1. XRD patterns of Nb–Al–N films with various aluminum content (a) and the enlarged XRD pattern of the film at 29.0 at% aluminum (b).

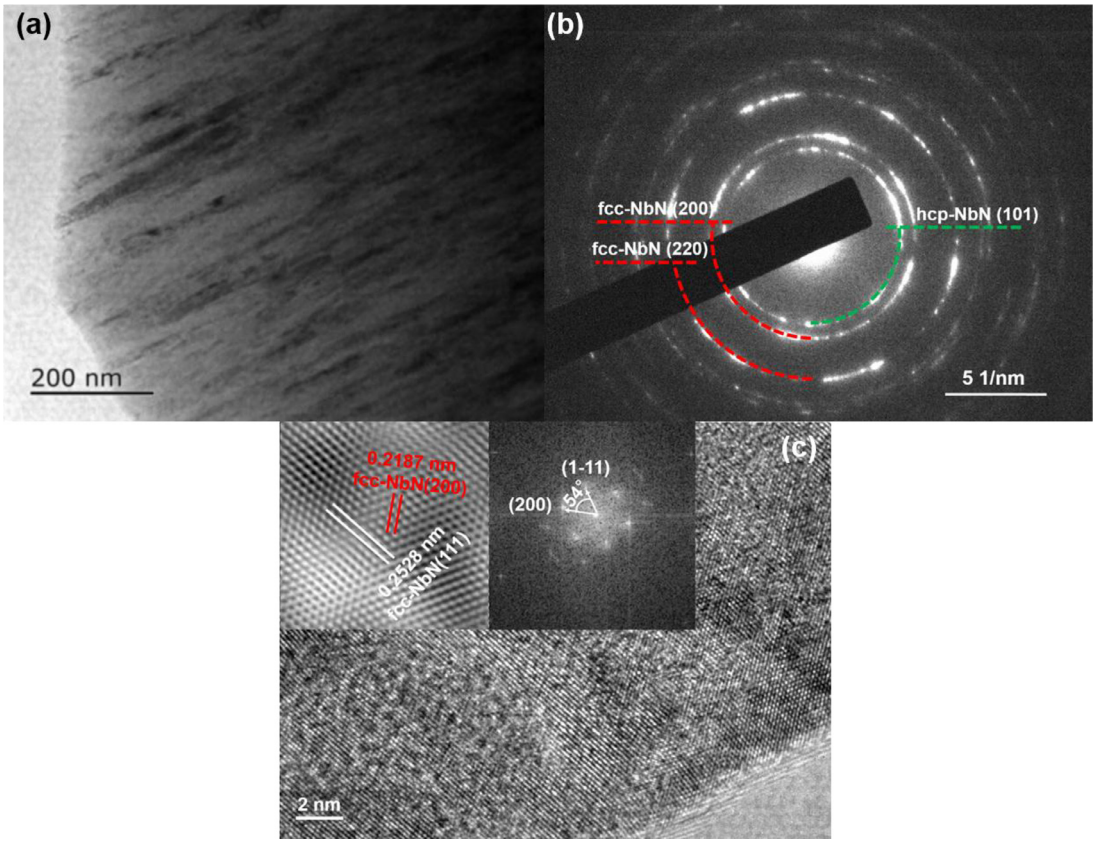

Fig. 2. Cross-sectional TEM image (a), its corresponding SAED pattern (b) and HRTEM image (c) of Nb–Al–N films with 22.3 at% aluminum.

umn width of the film based on the cross-sectional TEM image shown in Fig. 3(a). Fig. 3(b) exhibits the SAED pattern of the film with aluminum content of 29.0 at%, and the resultant diffraction rings can be referred to as the lattice planes of hcp-AlN (100), hcp-NbN (101) and fcc-NbN (200), (220) from inner to outer. Therefore, the increasing the aluminum content to 29.0 at% induces the appearance of hcp-AlN and a three-phase of fcc-NbN, hcp-NbN and hcp-AlN co-existing in the film. Fig. 3(c) and (d) are the HRTEM images of the film and its corresponding FFT and IFFT patterns with an aluminum content of 29.0 at%. As shown in Fig. 3(c), two types of lattice fringe with the value of 0.2187 and 0.1545 nm are detected, and the lattice fringe belongs to fcc-NbN (200) and (220), respectively, based on the JCPDF card 38-1155. The lattice spacing of the above lattice fringes is still smaller than the standard lattice spacing due to the formation of the substitutional solid solution of $(Nb_{1-x}Al_x)_{1-y}N_y$. The lattice fringes with values of 0.2513 and 0.2391 nm in Fig. 3(d) correspond to hcp-AlN (002) and (101), respectively, based on the JCPDF card 25-1133. The lattice spacing of the above lattice fringes is bigger than that of the standard lattice spacing owning to the solution of bigger niobium into the aluminum nitride lattice. The hcp-AlN (002) and (101) plane is detected in the FFT pattern,

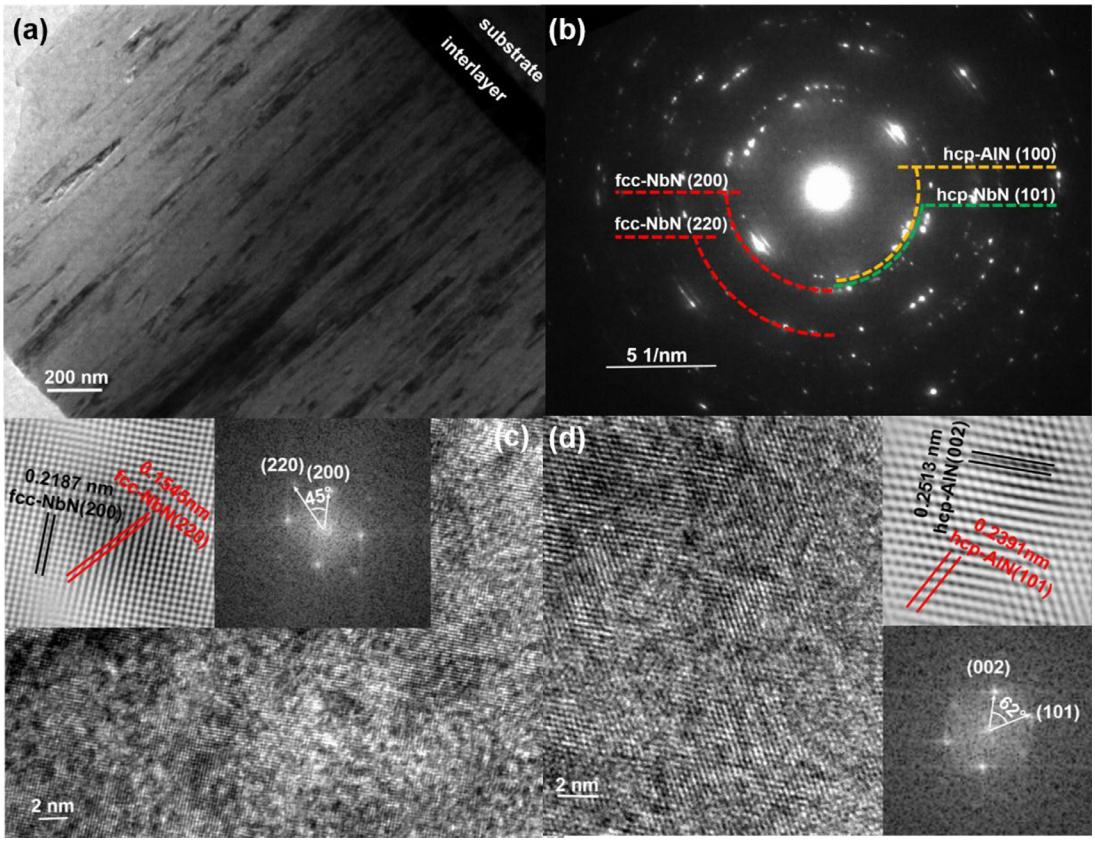

Fig. 3. Cross-sectional TEM image (a), its corresponding SAED pattern (b) and HRTEM image (c and d) of Nb–Al–N films with 29.0 at% aluminum.

and the angle between hcp-AlN (002) and (101) plane is 62°. This result is in good agreement with that of the lattice spacing.

Based on the results above, the Nb–Al–N films with the aluminum content below 22.3 at% shows a double phase of fcc-NbN and hcp-NbN, and it is the substitutional solid solution of fcc-$(Nb_{1-x}Al_x)_{1-y}N_y$ and hcp-$(Nb_{1-x}Al_x)_{1-y}N_y$. A further increase in the content of aluminum induces the formation of a third phase hcp-AlN because the niobium nitride lattice could not consume all aluminum atoms deposited into the film; hence, the film is a substitutional solid solution of fcc-$(Nb_{1-x}Al_x)_{1-y}N_y$, hcp-$(Nb_{1-x}Al_x)_{1-y}N_y$ and hcp-$(Al_{1-x}Nb_x)_{1-y}N_y$.

3.2. Mechanical and tribological properties at room temperature

Fig. 4 shows the compressive residual stress of Nb–Al–N films with varying aluminum content. The surface profile of the film is also shown as an inset. The binary niobium nitride film is in compression as can be seen in Fig. 4, and its value is ~−1.0 GPa. The compressive residual stress of binary aluminum nitride film deposited under the same conditions is ~−0.3 GPa. The incorporation of aluminum into niobium nitride matrix induces the compressive residual stress to rise rapidly from ~−1.3 GPa with 7.4 at% aluminum to ~−3.3 GPa with 22.3 at% aluminum; this is as a result of solid solution of aluminum. As the content of aluminum increases further, the compressive residual stress of films is reduced due to the emergence of aluminum nitride phase in the Nb–Al–N films.

Fig. 5 shows the hardness and elastic modulus of Nb–Al–N films with various aluminum content. The hardness of binary niobium nitride and aluminum nitride films are ~29 and ~21 GPa, respectively. The incorporation of aluminum into niobium nitride matrix results in the increase in hardness from ~32 GPa with 7.4 at% aluminum to ~37 GPa with 22.3 at% aluminum, solid solution strengthening and increase in compressive residual stress are the main reasons for such increases. The presence of aluminum nitride phase as a result of a further increase in aluminum content decreases the hardness of Nb–Al–N films from ~32 GPa with 29.0 at% aluminum to ~29 GPa with 38.3 at% aluminum, in spite of the existence of solid solution strengthening [18].

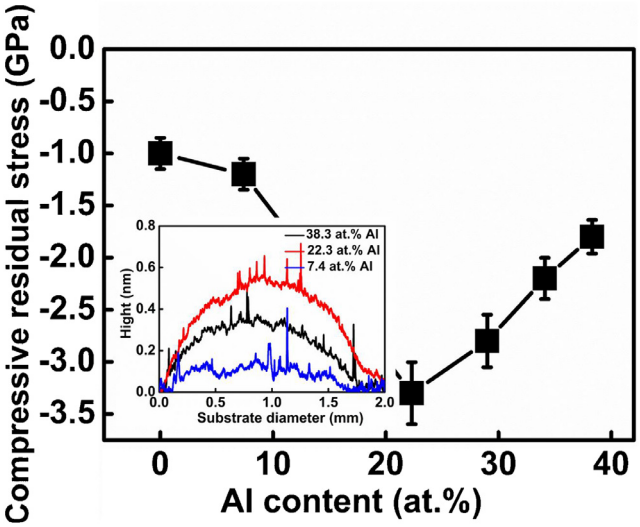

Fig. 4. Compressive residual stress and surface profile of Nb–Al–N films with various aluminum content.

The elastic modulus of the binary niobium nitride and aluminum nitride films are ~320 and ~260 GPa, respectively. Even though the factors that influence hardness and elastic modulus are entirely different, they have similar trends. The decrease in interatomic distance induced by the solution of aluminum leads to an increase in elastic modulus of Nb–Al–N films from ~340 GPa with 7.4 at% aluminum to ~350 GPa

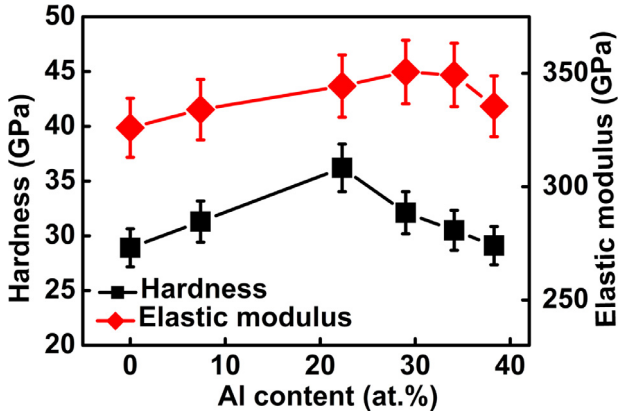

Fig. 5. Hardness and elastic modulus of Nb–Al–N films with various aluminum content.

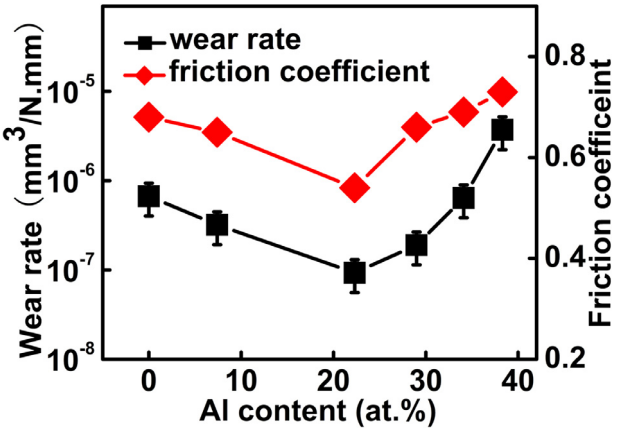

Fig. 6. Wear rate (*WR*) and average friction coefficient (μ) of Nb–Al–N films with various aluminum content at room temperature (RT).

with 34.1 at% aluminum. The presence of aluminum nitride phase in the films as a result of a further increase in aluminum content reduces the elastic modulus of the film due to the low elastic modulus of aluminum nitride phase.

Fig. 6 shows the wear rate (*WR*) and the friction coefficient (μ) of Nb–Al–N films with various aluminum content at room temperature (RT). For the binary niobium nitride and aluminum nitride films, the values of their *WR* are ~6.7×10^{-7} and ~4.2×10^{-5} mm^3/N.mm respectively; and their μ values are 0.68 and 0.83, respectively. The incorporation of aluminum into niobium nitride matrix reduces both *WR* and μ from ~3.2×10^{-7} mm^3/N mm and 0.65 with 7.4 at% aluminum to ~9.3×10^{-8} mm^3/N mm and 0.54 with 22.3 at% aluminum, respectively. But a further increase in Al content increases the *WR* and μ to maximum values of ~3.7×10^{-6} mm^3/N mm and 0.73 with 38.3 at% aluminum, respectively.

The adhesion force of the films has a strong influence on the nano/micro-friction results and was measured using the nano-indentation with the load of 4 mN. The result shows that the adhesion force of the Nb–Al–N films regardless of aluminum content in the films is ~0.1 mN. Therefore, the aluminum content has a limited effect on the adhesion force of the films and the *WR* and μ might influenced by some other factors. The addition of aluminum into transition metal nitride films can release the tensile and shear stresses induced by the counterpart during wear test according to our previous studies [10,19]. To some extent, it can retard the generation of cracks on the surface of the wear track and reduce the interaction of the film with the counterpart. Besides this, there is usually a correlation between mechanical and tribological properties at RT. As reported [1,22], the increase

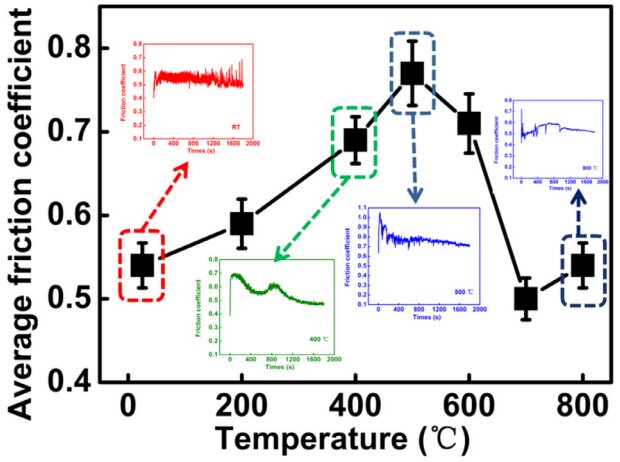

Fig. 7. Friction coefficient curves and μ of Nb–Al–N film at 22.3 at% aluminum with different testing temperatures.

in hardness also leads to a relatively small real contact area with the counterpart. Consequently, the film with high hardness value usually exhibits low *WR*. The reduction in *WR* and μ values are attributed to the increase in aluminum content of the Nb–Al–N films with aluminum content<22.3 at%, and the increase in hardness also results in improving the *WR* value. However, the appearance of aluminum nitride phase is responsible for the sharp rise in *WR* and μ of the Nb–Al–N films with aluminum content>22.3 at%. Besides this, the decrease in hardness of the film with aluminum content>22.3 at% also attributes to the increase in *WR*.

3.3. Tribological properties at elevated temperatures

The Nb–Al–N film with 22.3 at% aluminum which exhibits the lowest μ and *WR* values at RT, is chosen for the evaluation of its elevated temperature tribological properties. Friction coefficient curves and μ of Nb–Al–N film with the aluminum content of 22.3 at% at different test temperatures against Si_3N_4 counterpart is shown in Fig. 7. The test temperature affects the friction coefficient curve and μ as can be seen in Fig. 7. There is a marginal change in the friction coefficient value of the film against testing time. From RT to 200 °C, μ is relatively low with a value of ~0.57. Between 200 to 500 °C, fluctuations in friction coefficient vs. testing time is detected and the value of μ increases gradually. When the test temperature is increased further to 700 °C, fluctuations in friction coefficient vs testing time still exist, but there is a decline in the μ value. A constant μ value of about 0.50 is attained when the temperature is increased from 700 °C to 800 °C.

Apart from the frictional property, another essentail feature of transition metal nitride (TMN) films is their ability to resist wear. A Two-Dimensional and Three-Dimensional profiles of wear tracks at different testing temperatures are shown in Fig. 8 to investigate the wear property of the Nb–Al–N film with 22.3 at% aluminum. As shown in Fig. 8(a), after the wear test at RT, visible scratches appear on the surface of wear track, and copious amounts of wear debris were detected on the region near the center of the wear track, indicating the formation of a third body between the film and the counterpart during the wear tests. The wear track has an approximate width of 300 μm, and a depth of ~2 μm. From Fig. 8(b), as the testing temperature increases to about 200 °C, the adhesive wear debris disappeared in the wear track though there exist some few scratches. The wear track in Fig. 8(a) appears rougher as compared to the wear track in Fig. 8(b). The width of the track is ~300 μm with an approximate depth of 0.2 μm. Increasing the test temperature to 500 °C (as shown in Fig. 8(c)), the adhesive debris reappeared on both sides of the wear track, and the rough surface is similar to that of RT. The wear track has an approximate width of 400 μm, and a depth of

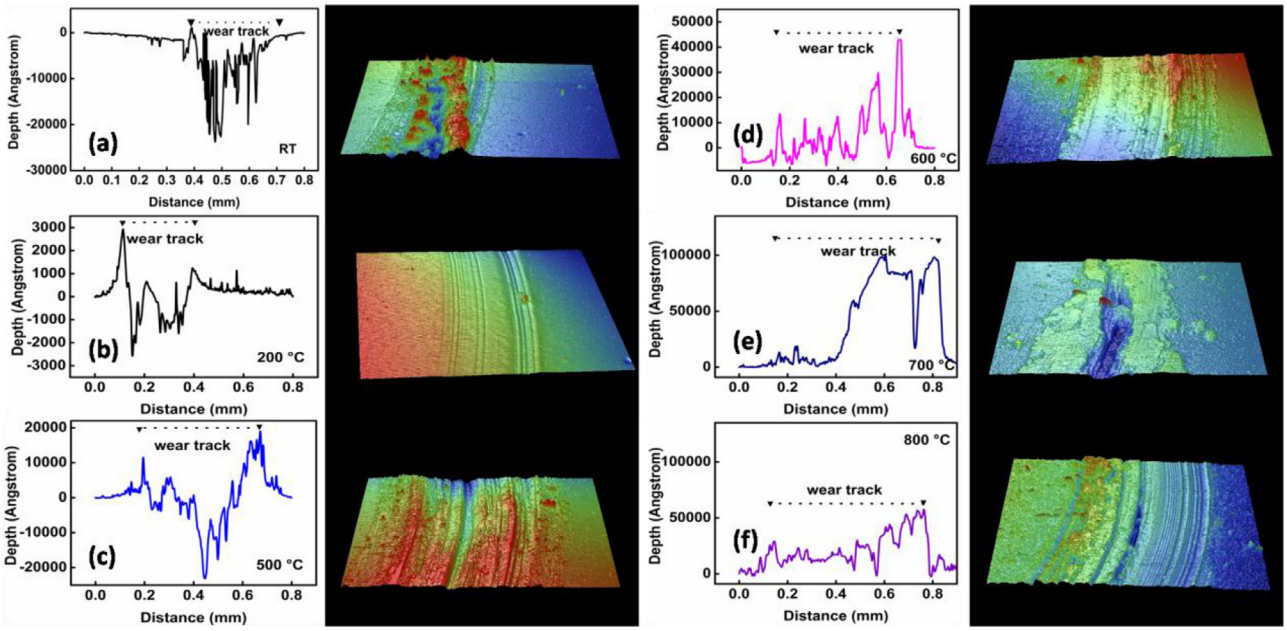

Fig. 8. Two-Dimensional and Three-Dimensional profiles of wear tracks at different testing temperatures: (a) RT, (b) 200 °C, (c) 500 °C, (d) 600 °C, (e) 700 °C, (f) 800 °C.

Table 2
Wear rate of Nb–Al–N film with 22.3 at% aluminum at different testing temperatures.

Testing temperature (°C)	Wear rate (mm^3/N mm)
RT	$(9.3 \pm 0.5) \times 10^{-8}$
200	$(6.7 \pm 0.3) \times 10^{-9}$
400	$(5.8 \pm 0.3) \times 10^{-8}$
500	$(1.4 \pm 0.1) \times 10^{-7}$
600	$-(3.7 \pm 0.2) \times 10^{-6}$
700	$-(7.2 \pm 0.3) \times 10^{-6}$
800	$-(9.4 \pm 0.5) \times 10^{-6}$

~2 μm. As shown in Fig. 8(d)–(f), the wear property is significantly improved when there is a further increase in test temperature. The width of the track is ~800 μm when the test temperature is above 600 °C. The surfaces height of all the wear tracks are higher than that of as-deposited films after wear test. At this period, the reconstruction of the worn area of the wear track happens.

Table 2 below shows the results obtained from the calculation of the *WR* of Nb–Al–N film with 22.3 at% aluminum. When the test temperature is below 200 °C, the *WR* drops rapidly from ~9.3×10^{-8} mm^3/N.mm at RT to ~6.7×10^{-9} mm^3/N mm at 200 °C, and then gradually increases from ~5.8×10^{-8} mm^3/N mm at 400 °C to ~1.4×10^{-7} mm^3/N mm at 500 °C. As the testing temperature increases further, the value of *WR* changes to a negative number. Besides this, the *WR* increases gradually with the increasing in test temperature.

Fig. 9(a) shows the TG profile of Nb–Al–N film with 22.3 at% aluminum. The temperature-dependent XRD patterns of the film are shown in Fig. 9(b) to investigate the changes in phase of the film after annealing at 400, 800, 1100, and 1200 °C. As can be seen, the sample weight is influenced by the test temperature slightly when the testing temperature is below 1100 °C. However, there is a linear increase in sample weight when the test temperature is above 1100 °C. The weight gained by the sample at elevated temperatures can be associated with oxidation reaction taken place [23–25] and the oxidation resistance temperature of the film is 1100 °C. From the XRD results (Fig. 9(b)), there is no change in phase of the film after annealing at 400 and 800 °C. Diffraction peaks corresponding to Nb_2O_5, rhombohedral Al_2O_3 (known as corundum) and cubic Al_2O_3 emerge when the test temperature is above 1100 °C.

The phenomenon of tribo-chemical reaction induced by the counterpart during the wear test is universal for transition metal nitride under un-lubricated sliding test. The elemental compositions of the wear track and unworn surface at different testing temperatures are shown in Table 3 to investigate the elemental redistribution after tribological test at elevated temperatures. As shown in Table 3, the niobium and aluminum content in the unworn area is independent of the testing temperature, and its value remains of ~29 and ~22 at%, respectively. However, the oxygen content of the unworn surface increases slightly from ~2.1 at% at RT to ~3.9 at% at 800 °C, with a corresponding dropping in nitrogen content from ~46.6 at% at RT to ~45.6 at% at 800 °C. Surface adsorption and measurement error might contribute to the increase in oxygen content since the oxidation resistance temperature of the film at 22.3 at% aluminum is 1100 °C. Besides this, the aluminum atom could diffuse into the surface to form the dense amorphous alumina by reacting with the oxygen in the air at elevated temperature. The appearance of alumina on the surface of the film was considered as the main reason for improving the oxidation resistance temperature of the films due to its dense structure [16,20,21]. Therefore, this also could attribute to the slight increase in oxygen content in the unworn area. However, the oxygen content in the unworn area regardless of the testing temperature is below 5.0 at%, and could be ignored. Therefore, the chemical compositions on the unworn could be regarded almost like that of the as-deposited film. The testing temperature influences the chemical compositions on the wear track significantly. Silicon which might come from the counterpart is detected on the wear track of the film regardless of the testing temperatures, and its value is in the range of 0.2–1.3 at%. The oxygen content on the wear track initially decreases from ~5.7 at% at RT to ~3.1 at% at 200 °C, and then increases gradually to 30.7 at% as the testing temperature increase to 800 °C. When the testing temperature increases from RT to 500 °C, aluminum and nitrogen content is independent on the testing temperature, and its value is similar to that of the as-deposited film. However, a further increase in the testing temperature induces the increase in the aluminum content with a corresponding of the decline in nitrogen content; it suggests that the testing temperature above 500 °C leads to the diffusion of aluminum onto the surface of the wear track and forms certain oxide based tribophases.

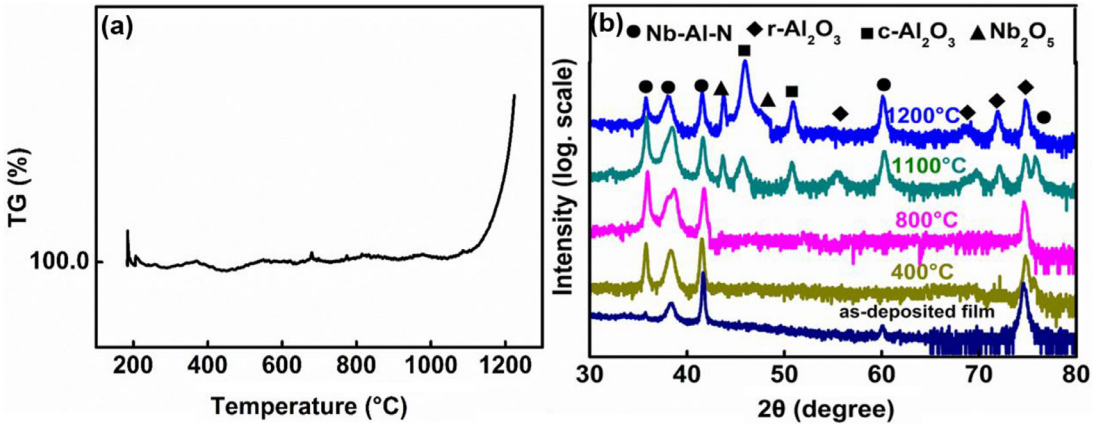

Fig. 9. TG profile of Nb–Al–N film with 22.3 at% aluminum (a), and the temperature-dependent XRD patterns of the film (b).

Table 3
The element compositions of the wear track and unworn surface at different testing temperatures.

Testing temperature (°C)	Chemical compositions on the unworn surface (at%)				Chemical compositions on the wear track (at%)				
	Niobinum	Aluminum	Nitrogen	Oxygen	Niobinum	Aluminum	Nitrogen	Oxygen	Silicon
RT	29.0 ± 1.5	22.3 ± 1.1	46.6 ± 2.3	2.1 ± 0.1	28.2 ± 1.4	22.1 ± 1.1	43.8 ± 2.2	5.7 ± 0.3	0.2 ± 0.1
200	29.2 ± 1.4	22.2 ± 1.1	46.3 ± 2.3	2.3 ± 0.1	26.7 ± 1.3	22.9 ± 1.1	46.5 ± 2.3	3.1 ± 0.2	0.8 ± 0.1
500	28.8 ± 1.4	22.1 ± 1.1	45.7 ± 2.3	3.4 ± 0.2	24.7 ± 1.2	21.8 ± 1.1	44.6 ± 2.2	8.4 ± 0.3	0.5 ± 0.1
600	28.2 ± 1.4	21.8 ± 1.1	46.2 ± 2.3	3.8 ± 0.2	17.5 ± 0.9	25.3 ± 1.1	35.1 ± 1.9	20.9 ± 1.0	1.2 ± 0.1
700	28.4 ± 1.4	22.1 ± 1.1	45.9 ± 2.3	3.6 ± 0.2	17.7 ± 0.9	27.4 ± 1.1	27.2 ± 1.7	26.9 ± 1.2	0.8 ± 0.1
800	28.6 ± 1.4	21.9 ± 1.1	45.6 ± 2.3	3.9 ± 0.2	17.5 ± 0.9	30.6 ± 1.1	18.9 ± 1.4	30.7 ± 1.5	1.3 ± 0.1

Raman spectra at different locations of the film with various testing temperatures are shown in Fig. 10 to investigate the presence of tribo-chemical reactions after the wear test. Fig. 10(a) shows the Raman spectra of the Nb–Al–N film with 22.3 at% aluminum after wear test at RT and the curve '1' is the as-deposited Raman spectrum which has two peaks at about 220 and 645 cm^{-1} corresponding to niobium nitride [23]. The wear track Raman spectrum is represented in curve '2' and has three peaks present at about 835, 870 and 1160 cm^{-1} besides the two peaks corresponding to niobium nitride; those three peaks belong to γ-Al_2O_3 and Nb_2O_5 [24–26]. During the wear test, the film interacts with moisture in the air in a complex chemical reaction forming the above tribo-phases. When the test temperature is increased to 200 °C, no peaks corresponding to niobium oxides or aluminum oxide are detected in the as-deposited film and wear track area, according to the Raman spectrum results shown in Fig. 10(b). The absence of γ-Al_2O_3 and Nb_2O_5 tribo-phase renders the wear track smooth and narrow. At this stage, the only environmental change is the reduction of moisture content in the service area as compared to RT. The absence of moisture at this temperature might lead to no tribo-chemical reaction taking. The wear track image and Raman spectra at different locations at a temperature of 500 °C are shown in Fig. 10(c). Increasing the test temperature significantly induces scratch on the wear track. Curve '1' is the as-deposited film's Raman spectrum at 500 °C, and two peaks corresponding to niobium nitride can still be observed, and some other peaks belonging to the oxides doed not appear, indicating that the film exhibits good thermal stability at 500 °C. Curve '2' is the Raman spectrum of the wear track, besides the peak corresponding to niobium nitride at 220 cm^{-1}, there are four other visible Raman peaks at about 315, 450, 835 and 1360 cm^{-1} belonging to γ-Al_2O_3 and a peak at about 690 cm^{-1} belonging to Nb_2O_5 [23–26]. Although the testing temperature is lower than the oxidation temperature of the film, friction heating generated by the interaction between the asperities on the surface and the counterpart during the wear test is responsible for the oxidation reaction in the wear track. A further increase in testing temperature to 600 °C, as shown in Fig. 10(d), the as-deposited film still exhibits good thermal stability and its Raman spectrum (curve '1') presents two peaks consistent with that of niobium nitride. The Raman spectrum (curve '2') from the wear track shows the peaks at 235 cm^{-1} belonging to Nb_2O_5 [23], peaks at 315, 1400 cm^{-1} belonging to γ-Al_2O_3 [24–26], and peaks at 414, 464, 560 cm^{-1} belonging to α-Al_2O_3 [27]. Besides this, two Raman peaks at about 220 and 645 cm^{-1} corresponding to niobium nitride [23] are still detected in the curve '2'. At this test temperature, a new α-Al_2O_3 tribo-phase which is the main component of the tribo-film is formed. At 700 °C, the as-deposited Nb–Al–N Raman spectrum (curve 1) is similar to that of niobium nitride. Observing from the wear track Raman spectrum of curve '2', peaks similar to that of curve '1' in Fig. 10(d) are still detected. An additional peak at about 835 cm^{-1} corresponding to α-Al_2O_3 [27] also emerges. It is evident that the amount of α-Al_2O_3 at this location is more than that of 600 °C.

Based on the results of TG, EDS and Raman spectra, the testing temperature has a little effect on the chemical compositions of the unworn film surface, and the unworn surface always exhibits a double phase of fcc-NbN and hcp-NbN. However, the chemical compositions and tribo-phases on the wear track are significantly influenced by the testing temperature. All possible tribo-phases formed on the wear track are shown in Table 4. As shown in Table 4, the wear debris Si_3N_4 from counterpart is always detected on the wear track regardless of testing temperatures, while the other tribo-phases of alumina and niobium oxide exhibits a significant temperature-dependent. Two kinds of oxide-based tribo-phase γ-Al_2O_3 and Nb_2O_5 appear on the wear track at RT. However, increasing the testing temperature to 200 °C, no visible oxide-based tribo-phases is detected. As the test temperature increases to 500 °C, γ-Al_2O_3 and Nb_2O_5 appear on the wear track again. For the wear track at a temperature >500 °C, the oxide-based tribo-phases detected are α-Al_2O_3, γ-Al_2O_3 and Nb_2O_5.

The film substrate might influence the tribological properties at elevated temperatures since it is not a very good oxidation resistance material. Fig. 11 illustrates the XRD patterns of the substrate at different annealing temperatures. As shown in Fig. 11, for the XRD pattern of AISI 304 SS at RT, three peaks corresponding to γ phase at ~43°, ~44°

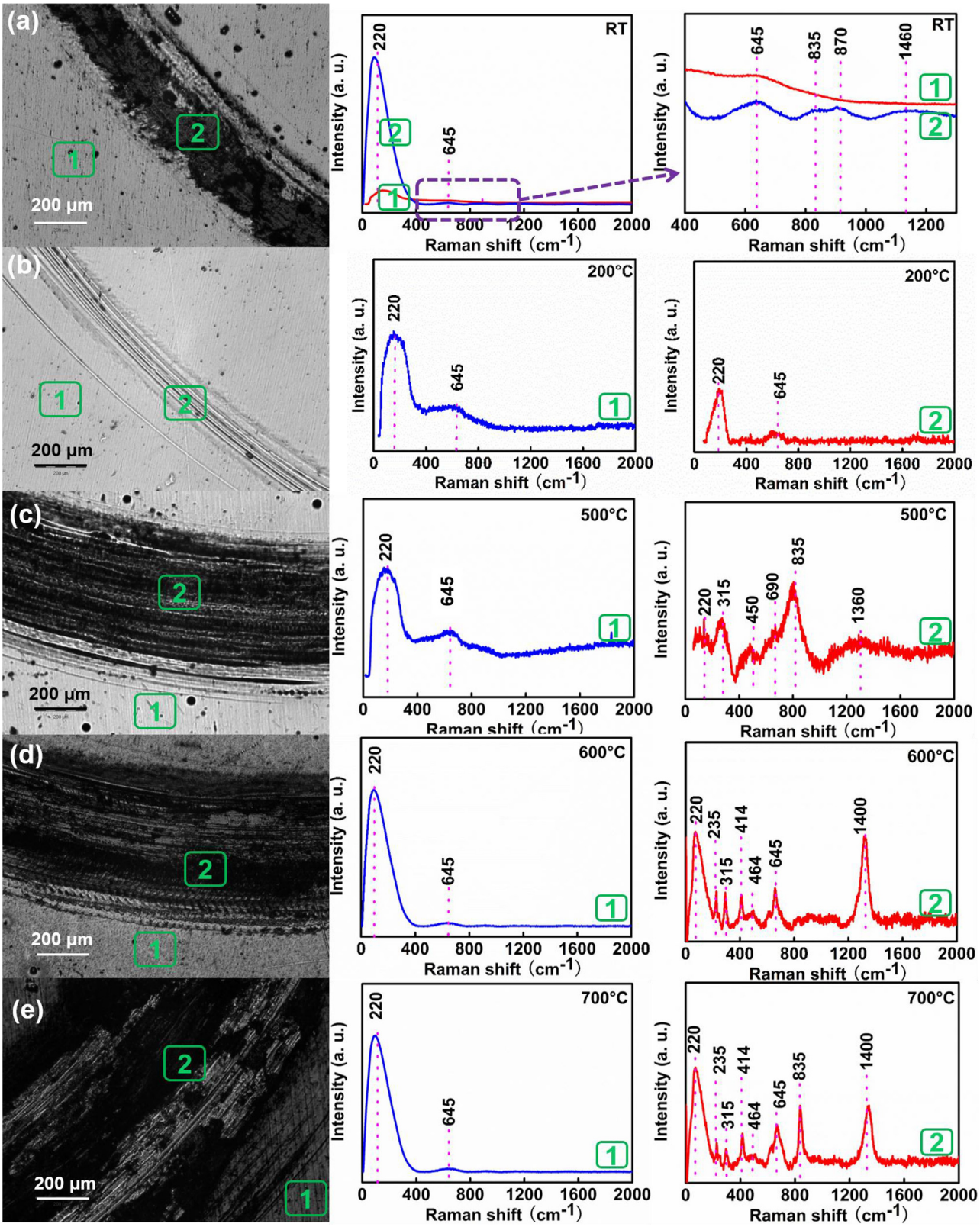

Fig. 10. Raman spectra of the wear track of Nb–Al–N film with 22.3 at% aluminum after different testing temperatures wear test: (a) as-deposited film (curve 1) and the wear track (curve 2) of the film at RT; (b) as-deposited film (curve 1) and the wear track (curve 2) of the film at 200 °C; (c) as-deposited film (curve 1) and the wear track (curve 2) of the film at 500 °C; (d) as-deposited film (curve 1) and the wear track (curve 2) of the film at 600 °C; (e) as-deposited film (curve 1) and the wear track (curve 2) of the film at 700 °C.

Table 4
The tribo-phases formed on the wear track at different testing temperatures.[a]

Tribo-phases				
	From tribo-chemical reaction		From counterpart	
Testing temperature (°C)	γ-Al_2O_3	α-Al_2O_3	Nb_2O_5	Si_3N_4
RT	√	×	√	√
200	×	×	×	√
500	√	×	√	√
600	√	√	√	√
700	√	√	√	√
800	√	√	√	√

[a] √: tribo-phase is detected on the wear track, ×: tribo-phase is not detected on the wear track.

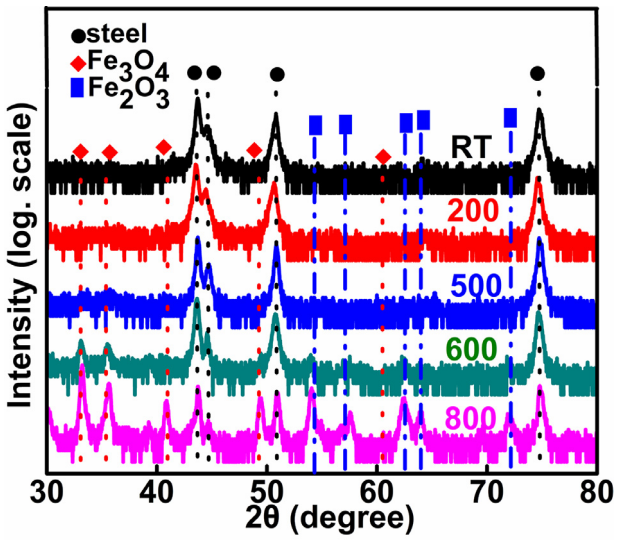

Fig. 11. XRD patterns of the substrate at different annealing temperatures.

and ~50° and one peak corresponding to δ phase at ~75° are detected. The substrate exhibits an excellent oxidation resistance property at temperatures <500 °C, since its XRD patterns at temperatures <500 °C still present four diffraction peaks similar to that of AISI 304 SS at RT. The substrate has a little effect on the tribological properties of the films at this period. However, a further increasing in the temperature above 600 °C induces the appearance of iron oxide phase and the substrate is oxidized. The softening of the substrate might cause an undesirable effect on the tribological properties of the hard brittle Nb–Al–N films. However, no obvious crack is detected on the surface of the wear track at temperatures >600 °C because of the relatively low load in our wear test and the appearance of soft niobium oxide. Besides this, testing temperature above 600 °C induces the reconstruction of the wear track and the surfaces height of all the wear tracks are higher than that of as-deposited films. The higher surface height of the wear track could eliminate the impact of substrate softening. Although the phase of the substrate is influenced by the temperature significantly, the substrate has a limited effect o on the elevated temperature tribological properties of the Nb–Al–N film with 22.3 at% aluminum.

Based on above analyses, during the wear test at RT, the asperities in the film surface first comes into contact with the counterpart, they are crushed by the frictional load and the shredded asperities move along the counterpart in the process scratching the film's surface. Moreover, γ-Al_2O_3 tribo-phase is formed under the action of the counterpart and this phase was reported to exhibit a porous structure [14]. This tribo-phase is easily crushed by the frictional load, and the interaction between the wear track and counterpart is further intensified. The main wear mechanism is adhesive wear with an accompanying oxidation wear. At this stage, the *WR* is relatively high with a value of $\sim 9.3\times10^{-8}$ mm^3/N mm and μ is relatively low with a value of 0.54. Increasing the testing temperature to 200 °C, the disappearance of γ-Al_2O_3 and Nb_2O_5 tribo-phases contributes to the wear track becoming smooth and narrow. The main wear mechanism is polishing wear and the wear property is improved compared to that of RT. The value of μ remains stable, while *WR* is reduced because of the disappearance of γ-Al_2O_3 at this stage. When the test temperature is between 200-500 °C, friction heating results in the oxidation reaction, γ-Al_2O_3 and Nb_2O_5 tribo-phases re-emerge. Consequently, both μ and *WR* gradually increases and the main wear mechanism changes to oxidation wear accompanying an adhesive wear. The high service temperature induces phase transition from porous γ-Al_2O_3 to dense α-Al_2O_3 structure when the test temperature is further increased. The α-Al_2O_3 is known as corundum and exhibits a high hardness. The adhesive tribo-film improves the surface hardness of the wear track, and the wear track exhibits a higher load carrying capacity. Hence, it is impossible for the surface to be worn away by the counterpart. Moreover, the formation of α-Al_2O_3 reconstructed the worn-out area of the wear track because the molar volume of α-Al_2O_3 (25.8 cm^3/mol) is much higher than that of NbN (12.6 cm^3/mol). Therefore, testing temperature above 600 °C induces the reconstruction of the wear track and the surfaces height of all the wear tracks are higher than that of as-deposited films.

4. Conclusion

Niobium aluminum nitride (Nb–Al–N) films with various aluminum content were deposited using a reactive magnetron system, and the crystal structure, mechanical and tribological properties were investigated. The main results showed as follows:

(1) Nb–Al–N films at <22.3 at% aluminum exhibited a double phase of face-centered cubic (fcc) NbN and hexagonal close-packed (hcp) NbN. At this period, aluminum atoms were dissolved into the fcc and hcp niobium nitride lattice and formed the substitutional solid solution of fcc-$(Nb_{1-x}Al_x)_{1-y}N_y$ and hcp-$(Nb_{1-x}Al_x)_{1-y}N_y$. A further increase in the content of aluminum induced the formation of a third phase of hcp-AlN because the solution of aluminum into niobium nitride lattice could not consume all aluminum atoms deposited on the film, and the film was the substitutional solid solution of fcc-$(Nb_{1-x}Al_x)_{1-y}N_y$, hcp-$(Nb_{1-x}Al_x)_{1-y}N_y$ and hcp-$(Al_{1-x}Nb_x)_{1-y}N_y$.

(2) The incorporation of aluminum into niobium nitride matrix resulted in a sharp rise in hardness from ~29 GPa with 0 at% aluminum to ~37 GPa with 22.3 at% aluminum, which was attributed to solid solution strengthening and increase in compressive residual stress. The appearance of the aluminum nitride phase decreased the hardness from ~32 GPa with 29.0 at% aluminum to ~29 GPa with 38.3 at% aluminum.

(3) When the aluminum content was below 22.3 at%, the wear rate (*WR*) and friction coefficient (μ) dropped gradually and had minimum values of $\sim 9.3\times10^{-8}$ mm^3/N mm and 0.54 with 22.3 at% aluminum, respectively. The appearance of the aluminum nitride phase which was as a result of an increase in the content of aluminum increased the *WR* and μ to maximum values of $\sim 3.7\times10^{-6}$ mm^3/N mm and 0.73, respectively, with 38.3 at% aluminum.

(4) From RT to 800 °C, the Nb–Al–N film with 22.3 at% aluminum film exhibited significant temperature-dependent tribological properties: when the testing temperature was below 200 °C, μ remained stable, and *WR* decreased significantly because of the disappearance of γ-Al_2O_3 and Nb_2O_5 tribo-phases. Increasing the testing temperature from 200 °C to 500 °C, frictional heating induced the emergence of γ-Al_2O_3, which resulted in the intensified interaction between wear track and the counterpart and the subsequent increase of μ and *WR*. Increasing the testing temperature further, high service temperature induced phase transition from porous γ-Al_2O_3 to dense a α-Al_2O_3.

The formation of α-Al_2O_3 reconstructed the worn-out area of the wear track at this period.

Declaration of interests

The authors declare that they have no known competing financial interests or personal relationships that could have appeared to influence the work reported in this paper.

Acknowledgments

Supported by National Key R&D Program of China (No. 2016YFB1100103), National Natural Science Foundation of China (51374115, 51574131, 51801081), China Postdoctoral Science Foundation (2018M632251), Research Fund of Jiangsu University of Science and Technology (1062931609) and Jiangsu University of Science and Technology undergraduate innovative entrepreneurship training pro gram. The authors also would like to thank Jing Luan for her valuable help in improving our manuscript.

References

[1] A. Voevodin, C. Muratore, S. Aouadi, Hard coatings with high temperature adaptive lubrication and contact thermal management: review, Surf. Coat. Technol. 257 (2014) 247–265.
[2] A. Erdemir, G. Ramirez, O. Eryilmaz, B. Narayanan, Y. Liao, G. Kamath, S. Sankaranarayanan, Carbon-based tribofilms from lubricating oils, Nature 536 (2016) 67–71.
[3] H. Ju, L. Yu, S. He, I. Asempah, J. Xu, Y. Hou, The enhancement of fracture toughness and tribological properties of the titanium nitride films by doping yttrium, Surf Coat Technol. 321 (2017) 57–63.
[4] H. Ju, S. He, L. Yu, I. Asempah, J. Xu, The improvement of oxidation resistance, mechanical and tribological properties of W_2N films by doping silicon, Surf. Coat. Technol. 317 (2017) 158–165.
[5] H. Ju, L. Yu, D. Yu, I. Asempah, J. Xu, Microstructure, mechanical and trobological properties of TiN-Ag films deposited by reactive magnetron sputtering, Vacuum 141 (2017) 82–88.
[6] Y. Zhao, X. Peng, T. Fu, C. Huang, H. Xiang, N. Hu, C. Yan, Investigation of mechanical behaviour of amorphous aluminium nitride. Mater. https://doi.org/10.1016/j.mtla.2018.07.011
[7] P Ren, K Zhang, S Du, Q Meng, X He, S Wang, M Wen, W Zheng, Toughness enhancement and tribochemistry of the Nb-Ag-N films actuated by solute Ag, Acta Mater. 137 (2017) 1–11.
[8] H. Ju, D. Yu, J. Xu, L. Yu, Y. Geng, T. Gao, G. Yi, S. Bian, J. Vac, Microstructure, mechanical, and tribological properties of niobium vanadium carbon nitride films, Sci. Technol. A 36 (2018) 031511–031517.
[9] W. Lengauer, M. Bohn, B. Wollein, K. Lisak, Phase reactions in the NbN system below 1400°C, Acta Mater. 48 (2000) 2633–2638.
[10] H. Ju, P. Jia, J. Xu, L. Yu, Y. Geng, Y. Chen, M. Liu, T. Wei, The effects of adding aluminum on crystal structure, mechanical, oxidation resistance, friction and wear properties of nanocomposite vanadium nitride hard films by reactive magnetron sputtering, Mater. Chem. Phys. 215 (2018) 368–375.
[11] H. Ju, N. Ding, J. Xu, L. Yu, I. Asempah, J. Xu, G. Yi, B. Ma, Crystal structure and the improvement of the mechanical and tribological properties of tungsten nitride films by addition of titanium, Surf. Coat. Technol. 345 (2018) 132–139.
[12] H. Ju, D. Yu, L. Yu, D. Ning, J. Xu, X. Zhang, Y. Zheng, L. Yang, X. He, The influence of Ag contents on the microstructure, mechanical and tribological properties of ZrN-Ag films, Vacuum 148 (2018) 54–61.
[13] H. Ju, X. He, L. Yu, J. Xu, The microstructure and tribological properties at elevated temperatures of tungsten silicon nitride films, Surf. Coat. Technol. 326 (2017) 255–263.
[14] A.V. Richthofen, R. Cremer, M. Witthaut, R. Domnick, D. Neuschütz, Composition, binding states, structure, and morphology of the corrosion layer of an oxidized $Ti_{0.46}Al_{0.54}N$ film, Thin Solid Films 67 (1998) 1109–1111.
[15] H. Sheng, F. Zhang, S. Veprek, Decomposition mechanism of Al1–xSixNy solid solution and possible mechanism of the formation of covalent nanocrystalline AlN/Si3N4 nanocomposites, Acta. Mater. 56 (2008) 968–976.
[16] P. Mayrhofer, D. Sonnleitner, M. Bartosik, D. Holec, Structural and mechanical evolution of reactively and non-reactively sputtered Zr-Al-N thin films during annealing, Surf. Coat. Technol. 244 (2014) 52–56.
[17] V. Ivashchenko, S.. Dub, P. Scrynskii, A. Pogrebnjak, O. Sobol', G. Tolmacheva, V. Rogoz, A. Sinel'chenko, J. Super. Mater 38 (2016) 103–113.
[18] R. Franz, M. Lechthaler, C. Polzer, C. Mitterer, Structure, mechanical properties and oxidation behaviour of arc-evaporated NbAlN hard coatings, Surf. Coat. Technol. 204 (2010) 2447–2453.
[19] J. Xu, H. Ju, L. Yu, Microstructure, oxidation resistance, mechanical and tribological properties of MoAlN films by reactive magnetron sputtering, Vacuum 103 (2014) 21–27.
[20] J. Musil, Hard nanocomposite coatings: Thermal stability, oxidation resistance and toughness, Surf. Coat. Technol. 207 (2012) 50–65.
[21] J. Lin, B. Mishra, J. Moore, W. Sproul, A study of the oxidation behavior of CrN and CrAlN thin films in air using DSC and TGA analyses, Surf. Coat. Technol 202 (2007) 3272-2383.
[22] Y. Wang, S. Zhang, Toward hard yet tough ceramic coatings, Surf. Coat. Technol. 258 (2014) 1–16.
[23] D. Stone, J. Migas, A. Martini, T. Smith, C. Muratore, A. Voevodin, S. Aouadi, Adaptive NbN/Ag coatings for high temperature tribological applications, Surf. Coat. Technol. 206 (2012) 4316–4321.
[24] M. Baronskiy, A. Rastorguev, A. Zhuzhgov, A. Kostyukov, O. Krivoruchko, V. Snytnikov, Photoluminescence and Raman spectroscopy studies of low-temperature γ-Al_2O_3 phases synthesized from different precursors, Opt. Mater. 53 (2016) 87–93.
[25] R. Pereira, F. Aquino, A. Ferrier, P. Goldner, R. Gonçalves, Nanostructured rare earth doped Nb_2O_5: Structural, optical properties and their correlation with photonic applications, J. Lumin. (2015) 170.
[26] Y. Liu, B. Cheng, K.K. Wang, G.P. Ling, J. Cai, C.L. Song, G.R. Han, Study of Raman spectra for γ-Al_2O_3 models by using first-principles method, Solid State Commun. 178 (2014) 16–22.
[27] P. Li, M. Lei, W. Tang, Raman and photoluminescence properties of α-Al_2O_3 microcones with hierarchical and repetitive superstructure, Mater. Lett. 64 (2010) 161–163.